þÿ R a i n f a l l v e g e t a t i o n i n t e r a c t i o n r e g u l a t e s t e m p e r anomalies during extreme dry events in the Horn of Africa

Abera, Temesgen Alemayehu

2018-08

þÿ A b e r a , T A , H e i s k a n e n , J H , P e l l i k k a , P K E & M a e d a , E E 2 0 1 8 , interaction regulates temperature anomalies during extreme dry events in the Horn of Africa '
, Global and Planetary Change , vol. 167 , pp. 35-45 . https://doi.org/10.1016/j.gloplacha.2018.05.002

http://hdl.handle.net/10138/235603
https://doi.org/10.1016/j.gloplacha.2018.05.002

Global and Planetary Change 167 (2018) 35–45

Contents lists available at ScienceDirect

Global and Planetary Change

journal homepage: www.elsevier.com/locate/gloplacha

Research article

Rainfall–vegetation interaction regulates temperature anomalies during extreme dry events in the Horn of Africa

Temesgen Alemayehu Abera[a,b,*], Janne Heiskanen[a,b], Petri Pellikka[a], Eduardo Eiji Maeda[c]

[a] Department of Geosciences and Geography, P.O. Box 68, FI-00014 University of Helsinki, Finland
[b] Institute for Atmospheric and Earth System Research, Faculty of Science, University of Helsinki, Finland
[c] Ecosystems and Environment Research Program, Faculty of Biological and Environmental Sciences, P.O. Box 65, FI-00014 University of Helsinki, Finland

ARTICLE INFO

Keywords:
Forest loss
Drought
LST anomaly
MODIS
TRMM
Horn of Africa

ABSTRACT

Climate–vegetation interaction can be perturbed by human activities through deforestation and natural extreme climatic events. These perturbations can affect the energy and water balance, exacerbating heat stress associated with droughts. Such phenomena are particularly relevant in the Horn of Africa, given its economic and social vulnerability to environmental changes. In this paper, we used 16-year time series (2001–2016) of remotely sensed environmental data with the objective of 1) clarifying how rainfall–vegetation interaction affects land surface temperature (LST) seasonality across the Horn of Africa, and 2) evaluating how this interaction affects LST anomalies during forest loss and drought events. Our results showed that vegetation seasonality follows rainfall modality patterns in 81% of the region. On the other hand, seasonality of daytime LST was negatively related to vegetation greenness patterns across ecoregions, and rainfall modality. LST varied more strongly in grasslands and shrublands than over other vegetation classes. Comparison of LST before and after forest loss in three selected areas (two in Ethiopia and one in Kenya) revealed an annual average increase in LST of 0.7 °C, 1.8 °C, and 0.2 °C after climate variability correction, respectively. The average increase in LST was relatively high and consistent during dry months (1.5 °C, 3 °C, and 0.6 °C). As expected, the rainfall anomalies during droughts (2010/2011, 2015, and 2016) were positively correlated with vegetation greenness anomalies. Nonetheless, the degree with which vegetation cover is affected by extreme rainfall events has a strong influence in regulating the impact of droughts on temperature anomalies. This highlights the importance of vegetation resilience and land cover management in regulating the impact of extreme events.

1. Introduction

The role of climate in the East African economy is particularly relevant compared with other parts of the world, due to the economy being highly dependent on agriculture (Blein et al., 2013). The health of climate–vegetation interaction in this region is therefore critical to sustaining the lives of millions of people. Recurrent droughts, however, pose a serious risk to food security. From 1900 to 2016, the Greater Horn of Africa alone experienced 36 drought events affecting > 150 million people, causing over 400,000 deaths and a total damage of USD 1,495,900,000 (EM-DAT: The Emergency Events Database, n.d.). The frequency of droughts have increased in the region following reduced spring precipitation over the last 30 years due to increase in westward extension of Indian-Pacific warm pool bringing warm and dry winds inhibiting rainfall (Williams and Funk, 2011). Future climatic projections suggest an increase in temperature in East Africa (Conway and Schipper, 2011; Anyah and Qiu, 2012). These projections together with the reduced precipitation trends in the region, drier conditions are expected in the coming century (Williams and Funk, 2011). This will cause further stress on vegetation.

The impact of drought on vegetation productivity can vary depending on its magnitude, frequency, and duration. Drought events impact agricultural productivity and can cause reduction in yield and crop failure, leading to food shortage. Severe droughts can bring about extensive decline or collapse in the normal seasonal patterns giving rise to failures in the phenological cycle of plants as reported during Australia's 2002 drought (Ma et al., 2015). Drought stress limits the ability of plants to supply water to leaves for photosynthetic gas exchange and can ultimately result in extreme dryness and mortality (Choat et al., 2012). Though several studies have been done to investigate the links between drought and vegetation productivity (Zhao and Running, 2010; Meroni et al., 2017), less is known about how this relationship impacts the land surface temperature (LST) and causes warming anomalies in the Horn of Africa.

* Corresponding author at: Department of Geosciences and Geography, P.O. Box 68, FI-00014 University of Helsinki, Finland.
E-mail address: temesgen.abera@helsinki.fi (T.A. Abera).

https://doi.org/10.1016/j.gloplacha.2018.05.002
Received 29 September 2017; Received in revised form 25 March 2018; Accepted 17 May 2018
Available online 24 May 2018

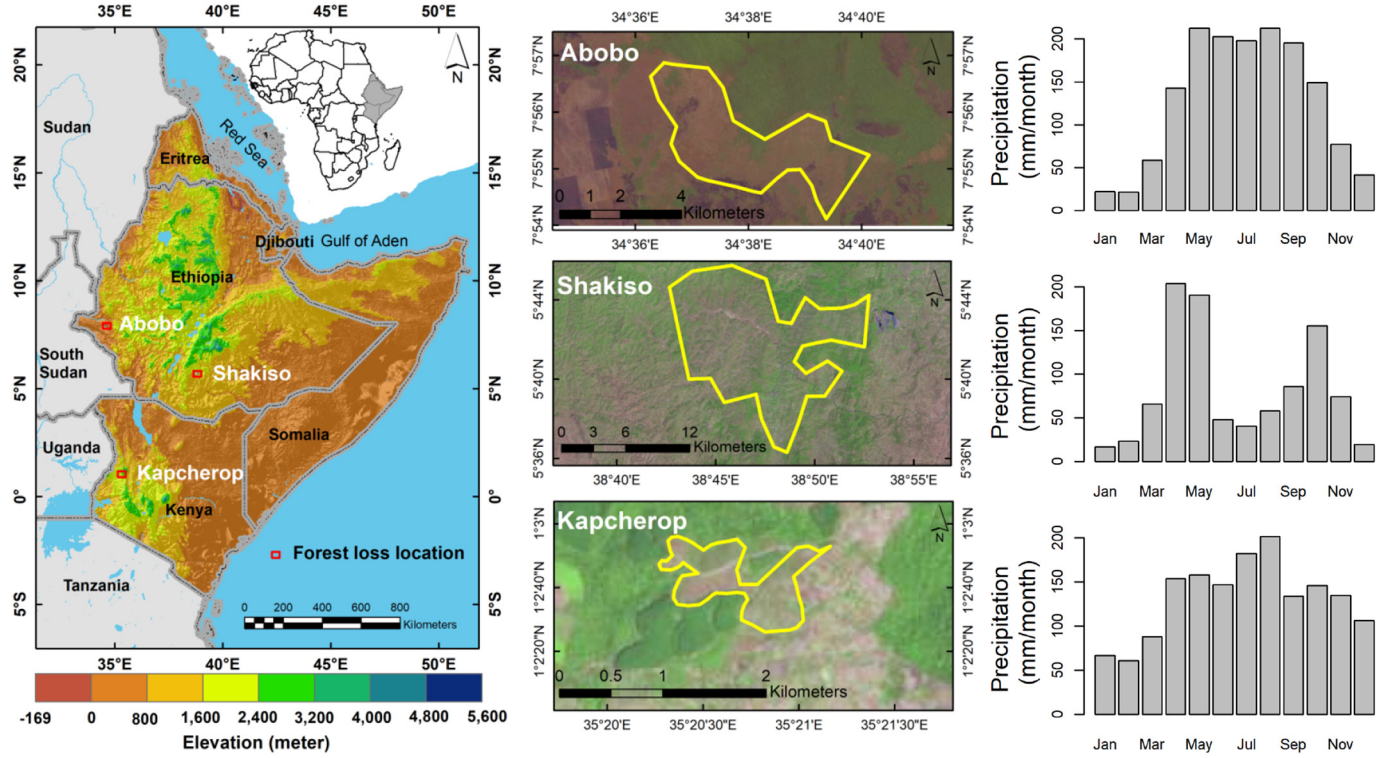

Fig. 1. Geographic location and elevation (GTOPO30 1 km) of Horn of Africa with forest loss locations presented. (Background image, Copernicus Sentinel data, January 2017). Precipitation information from TRMM43B3.

Vegetation cover can help to mitigate the impact of local warming related to drought. Vegetation suppresses the impact of local warming through increasing transpiration rates, which enhance transport of latent heat from the surface to the atmosphere, leading to surface cooling (Anderson et al., 2011). The surface roughness, which is related to the height of the vegetation, also favors surface cooling through facilitating the exchange of sensible and latent heat energy between the land surface and the atmosphere through creating turbulence that mixes the air and transports heat and water (Sud et al., 1988). Vegetation cover (such as forests) also has an important role in reducing the adverse impact of droughts through increasing the infiltration and storage capacity of soil, absorbing excess rainwater and releasing it during dry periods to replenish stream flows (Scott, 2005; EEA, 2015). Furthermore, forests play significant role in capturing atmospheric moisture by intercepting fog and cloud droplets through their volume, which in montane forests may enhance the water supply by providing additional moisture (Ellison et al., 2017).

Nonetheless, the land surface attributes are being modified due to the increasing influence of man on the environment through degrading terrestrial vegetation cover (in favor of agriculture, urbanization, fuel, timber, etc.). Forests in particular are facing significant changes. These changes can alter the energy, carbon, and water balance leading to further warming/cooling depending on the relative impacts of radiative (albedo) and non-radiative responses (evapotranspiration, surface roughness), which vary across the latitudes (Li et al., 2015). Based on satellite observation, Li et al. (2016) reported forest loss to have a warming impact in the tropics and a cooling effect in boreal regions. The warming in the tropics is attributed to the dominating impacts of the reduction in evapotranspiration rate and surface roughness (causing less heat convection), whereas the cooling in boreal regions is related to an increase in albedo. In contrast, forest gains are found to have the opposite effect, i.e., cooling in the tropics – mainly by driving away energy from the surface to the atmosphere through increased evapotranspiration and heat convection – and warming in boreal regions associated with decreased albedo (Bright et al., 2017; Li et al., 2016; Peng et al., 2014). At a global scale, impacts of forest cover changes on climate have been studied following different approaches (e.g. modeling, remote sensing, and in situ observations) (Davin and de Noblet-Ducoudre, 2010; Bright et al., 2017; Li et al., 2015). One important advantage of remote sensing based approaches is that they enable repeated sampling of large areas. This is particularly important in regions where in-situ measurements are lacking. Common to most remote sensing studies on forest loss impacts is the use of land cover data and threshold values to identify forest cover change (Li et al., 2016). The accuracy of the results can be affected by the input data used (land cover, LST), topography of forest loss area, choice of threshold values, and interannual climatic variability (Alkama and Cescatti, 2016). Therefore, further studies are needed at the regional and local level to examine the impacts of forest loss on LST by focusing on areas experiencing changes in forest cover, and by comparing before and after situations using relatively high resolution and long periods of data.

Furthermore, temporal aspects of the feedbacks between droughts, vegetation, and temperature are not yet fully understood. For instance, the role of vegetation phenology in regulating the impact of droughts is still unclear. It is therefore uncertain how the timing of extreme events affects the vulnerability of the regions to extreme events. Likewise, it is unclear how the interplay between vegetation resilience and drought events can affect the magnitude of temperature anomalies during extreme events. It is possible that severe but short extreme events cause lower temperature anomalies than moderate but long droughts. Clarifying these issues is critical for a better understanding of the biophysical processes taking place during droughts, and consequently to improve land surface models and management strategies.

The objective of this study was to investigate how rainfall–vegetation interactions affect LST anomalies during forest loss and drought events across the Horn of Africa using 16-years of data (2001–2016). To meet this objective, the following research questions were addressed: 1) How does rainfall–vegetation interaction affect seasonal patterns in temperature in the Horn of Africa? 2) What are the impacts of forest loss on temperature seasonality and anomalies? 3)

How does vegetation status/vigor affect LST anomalies during drought events?

1.1. Study area

The study area covered five countries in the Horn of Africa: Ethiopia, Eritrea, Djibouti, Somalia, and Kenya (Fig. 1). The region is characterized by a wide range of topographic, climatic, and ecological diversity. Elevation ranges from about 125 m below sea level in the Danakil Depression (Ethiopia) up to around 5199 m above sea level at Mount Kenya. Annual rainfall distribution varies from > 1500 mm in the highlands to < 200 mm in the lowlands. Much of the region shows a bimodal rainfall pattern under significant influence of the Intertropical Convergence Zone (Nicholson, 1996). Most portions of the region receive the main rainfall from March to May and a short period of rain from October to December. This short period of rain is characterized by high interannual variability associated with the El Niño–Southern Oscillation and the Indian Ocean Dipole (Bowden and Semazzi, 2007; Indeje et al., 2000).

Three main types of ecoregions (Somali-Masai, Afromontane, and Sudanian) with a dominantly arid and semi-arid climate characterize the region. The Somali-Masai ecoregion (mainly shrubland, grassland, and bushland) covers large parts of the low-lying region, while the Afromontane (forest) ecoregion covers small parts of the highlands of Ethiopia and Kenya. An extension of the Sudanian ecoregion (mainly grassland) also covers the western periphery of Ethiopia (see White, 1983 for details).

In sub-Saharan Africa, croplands are cleared at the expense of forest and native vegetation (Brink and Eva, 2009; Pellikka et al., 2013). In a recent study by Brink et al. (2014) in the Horn of Africa, 28% increase in croplands was recorded between 1990 and 2010, the yearly increase rate being 1.4%. The Abobo, Shakiso and Kapcherop are some of the areas experiencing forest loss in the region (Fig. 1). The Abobo forest loss area, which occupies the lowlands of Gambella region in Ethiopia, is covered by Sudanian woodland. It has mean elevation of around 568 m a.s.l, maximum temperature of 35 °C–40 °C and receives extended rainfall from March to November. The Shakiso forest loss site, on the other hand, is located in the vicinity of Shakiso town, in Oromia regional states of Ethiopia. The area has mean elevation of 1792 m a.s.l with an annual average temperature of 20 °C. It receives rainfall twice per year between March to May and September to November. Wooded grassland makes up most of the vegetation cover in this area. The Kapcherop forest loss area, which is one of the Afromontane forests in the highlands of Kenya, has mean elevation of around 2390 m a.s.l and annual average temperature around 16 °C. Tropical humid climate with extended rainfall (April to November) characterize the area (Fig. 1).

2. Material and methods

2.1. Remote sensing data and pre-processing

To characterize vegetation seasonality, we used monthly Enhanced Vegetation Index (EVI) (Huete et al., 2002) imagery from 2001 to 2016. The Moderate Resolution Imaging Spectroradiometer (MODIS) product used was the MCD43B1, which provides bidirectional reflectance distribution function (BRDF) model parameters for 8-day periods at 1 km spatial resolution (NASA LP DAAC, 2014). We first calculated nadir view reflectance factors considering a 45° solar zenith angle and nadir view angle for each 8-day product, therefore excluding the influence of sun-sensor geometry artifacts on the time series. Monthly averages for each band were then calculated and used to construct the monthly EVI imagery for the 16 years (2001–2016).

In characterizing vegetation condition using vegetation indices, removing the impact of non-vegetation signal is important to assess changes attributed only to vegetation. Thus, we preferred EVI over other indices (e.g., normalized difference vegetation index (NDVI)) since it is less affected by non-vegetation signal coming from background soil. Furthermore, atmospheric influence on the red band has been further reduced, which is additional advantage in terms of sensitivity to variations in the biophysical characteristics of vegetation (Gao et al., 2000; Huete et al., 2002). The EVI was calculated using the blue, red, and near-infrared (NIR) bands (Huete et al., 2002):

$$EVI = 2.5\frac{\rho_{NIR} - \rho_{red}}{\rho_{NIR} + 6 \times \rho_{red} - 7.5 \times \rho_{blue} + 1} \quad (1)$$

where ρ refers to BRDF corrected reflectance. The resultant product is less affected by atmospheric contamination, cloud cover is explicitly masked, and impacts of sun-sensor geometry are corrected.

LST refers to the skin or radiometric temperature at the surface (Jin and Dickinson, 2010). It differs from air temperature not only in its definition, but also in the way it is measured and its magnitude. Land heats and cools more quickly than air, and as a result, LST is higher (lower) during the day (night) than air temperature. Its magnitude is also affected by land surface properties (such as vegetation cover and surface albedo) and atmospheric interactions (Jin and Dickinson, 2010). Thus it is a key parameter in measuring energy fluxes between the land surface and atmosphere. The LST product chosen for the study was the MOD11A2 8-day composite at 1 km resolution. Radiance-based validation of this product indicated an accuracy better than one Kelvin in vegetation, soil, and lake areas in clear-sky conditions (Wan, 2015). LST values that are severely contaminated by clouds and heavy aerosols have been removed from this product and a quality control layer is provided for identification of good quality pixels (Wan, 2015). In this study, we have further removed cloud contaminated and bad quality pixels through assessment of the quality assessment flags. Once the images were filtered to allow only good quality pixels, monthly average LST from 2001 to 2016 was calculated. Furthermore, although the LST algorithm is fine-tuned to improve its effectiveness in desert regions, where the split-window algorithm normally shows poor performance, we masked these areas from our analysis (Hulley and Hook, 2009; Wan, 2015). We also preferred daytime LST over nighttime because much of the vegetation activity which affects LST (such as transpiration and photosynthesis) takes place during the daytime.

Rainfall was assessed using monthly data from the Tropical Rainfall Measuring Mission (TRMM) at 0.25° spatial resolution. The product used was the TRMM 3B43 version7, which combines the 3-hourly merged infrared estimates with rain gauge analysis from the monthly accumulated Global Precipitation Climatology Centre (GPCC) rain gauge analysis (GES DISC, NASA 2016). A summary of the remote sensing data is presented in Table 1. Furthermore, standardized

Table 1
Remote sensing data.

Data type	Sensor	Product	Version	Spatial resolution	Temporal resolution	Year	Reference
BRDF/Albedo model parameters	MODIS	MCD43B1	5	1 km	8-day composite	2001–2016	NASA LP DAAC, (2014)
LST	MODIS	MOD11A2	6	1 km	8-day composite	2001–2016	Wan, (2015)
Rainfall	TRMM	3B43	7	0.25°	Monthly	2001–2016	GES DISC, (2016)
Elevation		GTOPO30		1 km			USGS EDCDAAC, (2016)
Global Land Cover-SHARE				1 km		2014	Latham et al., (2014)
Global Forest Change	Landsat			30 m		2000–2014	Hansen et al., (2013)

anomalies for EVI, LST, and rainfall were calculated as follows:

$$X_{sd} = \frac{X - \mu}{\sigma} \quad (2)$$

where X_{sd} is the standardized anomaly; X is the value for the month; μ and σ are the mean and standard deviation over the 2001–2016 time period, respectively.

2.2. Identification of modality patterns and land–climate interactions

Unimodal and bimodal patterns, in our context, refers to rainfall (EVI) distribution with one and two local maxima (peaks), respectively. To identify and map the modality patterns for both rainfall and vegetation, we followed four steps. First, we resampled rainfall data to 1 km resolutions to match EVI data; then monthly climatology was calculated from the timeseries data (2001–2016). Second, a non-parametric locally weighted polynomial regression model (LOESS) was run to fit the seasonality curve. The model was combined with a peak identification function and applied in randomly chosen test pixels to determine peak identification and model parameters for the best fit. The function first identifies all local maxima from the rainfall climatology and then checks if the value is at least twice higher than the neighboring values. Then, if it meets this criterion, assigns the number of peak(s) for each pixel. We defined this criterion after testing its applicability in identifying rainfall peak(s) in the region by randomly choosing pixels from known unimodal and bimodal areas. This way, the function is constrained to ignore small fluctuations so that distinct local maxima can be identified. Third, once the best fit was obtained, the monthly climatology data were stacked sequentially (January–December) for both rainfall and EVI, and the modality was calculated for every pixel. Correlation between monthly climatology of rainfall and EVI was also checked using non-parametric Spearman's rank correlation.

To evaluate the influence of rainfall–vegetation interaction on LST, we selected representative samples (10 × 10 km), one from unimodal and another from bimodal area, for each of the three most common classes of natural vegetation cover (forest, grassland and shrubland) where EVI-rainfall interaction is strong (correlation coefficient ≥ 0.8).Average values of EVI and LST were then extracted from each sample area using the monthly climatology and plotted for unimodal and bimodal areas separately. Scatter plots of rainfall against EVI were classified using the corresponding LST value for each location to show how the three variables interact with each other. To identify how LST changes with changes in seasonality of vegetation across different vegetation classes, we used the monthly climatology data, standardized values to a common scale, and then calculated the slope of a linear regression between EVI (predictor) and LST (dependent variable) for each pixel.

2.3. Forest loss impact on land surface temperature

The impacts of forest loss on LST were assessed across three selected areas (Fig. 1) that underwent significant forest loss (> 90% of the area) between 2001 and 2016. For identifying the areas, we first narrowed down the search using Global Forest Change data (Hansen et al., 2013). The candidate areas were verified using high resolution imagery from Google Earth. Areas showing a mix of forest loss and gain, and areas that did not show deforestation according to high resolution imagery despite Global Forest Change data indicated loss, were excluded. Eventually, areas which were completely covered by forest at the beginning of the observation period but lost forest cover progressively towards the end of the observation period (> 95% for Ethiopian areas and > 85% for Kenyan area) were selected as forest loss areas covering 15 km^2, 160 km^2, and 1 km^2, respectively (Fig. 1).

To classify the before and after forest loss states, we used the period when 75% of the forest cover was intact as before forest loss state, and the period when forest cover was < 50% as after forest loss state, for all three areas. Then, average EVI and LST were calculated for both states using monthly climatology data.

We also analyzed dry months (January, February, March, and December) – defined in this study as months with < 100 mm of rain – separately to identify forest loss impact on LST anomalies. For this purpose, monthly anomalies of EVI and LST were calculated from the time series and the results were displayed as bar plots.

Moreover, we studied non-forest loss signal due to climatic variability by calculating the monthly average LST difference for the adjacent intact forest areas (< 5 km) using the corresponding periods (before and after forest loss) (Alkama and Cescatti, 2016) as follows:

$$\Delta LST = LST_b - LST_f \quad (3)$$

where ΔLST is change in LST due to climatic variability; $LST_b$is the average LST for the corresponding before forest loss period (2001–2008, 2001–2006, and 2001–2010); and LST_f is average LST after the forest loss period (2010–2016, 2008–2016, and 2012–2016) for areas 1, 2, and 3, respectively. In intact forest, where there was no forest loss, we assumed that change in LST comes mainly from climatic variability.

2.4. Drought impact on land surface temperature

Rainfall anomalies from two recent and strong drought years were selected (2010/2011, and 2015) (Dutra et al., 2013). For the 2011 drought, rainfall anomalies were detected since October 2010; thus we used 2010 (October–December) and 2011 (March–May) rainfall anomalies. Then for the same period, we calculated EVI and LST anomalies from the time series (2001–2016) using Eq. (2), and plotted rainfall and EVI anomalies classified by LST anomalies in order to understand their interaction. A similar approach was followed for the 2015 drought. Average LST anomalies over EVI and rainfall anomaly bins were calculated to quantitatively demonstrate their relative impact.

3. Results

3.1. Rainfall–vegetation interaction and its impact on daytime land surface temperature

The spatial patterns in rainfall and vegetation modality are presented in Fig. 2. The vegetation seasonal growth pattern followed the rainfall modality pattern in both unimodal and bimodal areas. Unimodal rainfall and EVI patterns were shown mainly in Ethiopia, whereas bimodal patterns were widely distributed across Kenya, Somalia, and the southern parts of Ethiopia. The rainfall modality showed 81% similarity with the EVI modality pattern. The disparity is distributed mainly in the humid parts of western Ethiopia. The correlation between rainfall and EVI showed that EVI and rainfall have a strong and positive correlation ($r > 0.7$) for most areas of significant relationship ($p < 0.05$) and this accounts for 78% of the total area (Fig. 2c).

Temperature showed a negative relationship with EVI and rainfall in all areas of shrubland, grassland, and forest, and the same relationship was observed across unimodal and bimodal patterns (Fig. 3). The daytime LST seasonality curve changes in the opposite phase to the EVI pattern for all vegetation classes. During the wet season, EVI reaches a local maximum and LST displays a local minimum. During dry periods, in contrast, LST displayed the local maximum for the corresponding EVI local minimum. The degree with which LST changes with EVI pattern, however, is higher in unimodal than bimodal areas.

For the same areas, the relationships between rainfall, EVI, and LST were studied using monthly time-series data (2001–2016) to understand how rainfall–EVI interaction affects LST (Fig. 4). The results show that when rainfall and EVI increase, LST decreases and vice versa for all vegetation classes (Fig. 4). Furthermore, this interaction is consistent for both unimodal and bimodal areas.

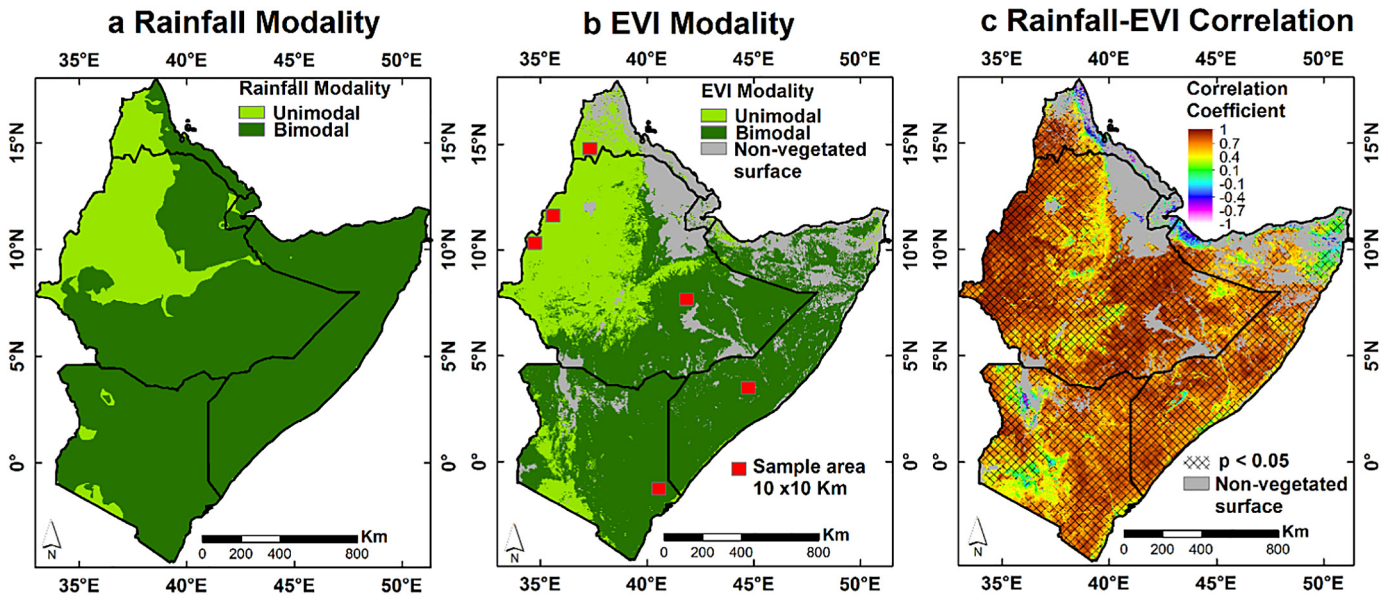

Fig. 2. Map showing a) modality of rainfall pattern, b) modality of EVI pattern, and c) rainfall– EVI correlation. Vegetation was masked using Global Land Cover data.

The spatial variability of the EVI–LST relationship is presented in Fig. 5. Daytime LST is negatively related to EVI in all areas, with a significant linear relationship ($p < 0.05$) (Fig. 5a). The slope of linear regression between LST (response variable) and EVI (predictor variable) shows that LST in grassland and shrubland changes more strongly (-1.9 to -4.9) than over other vegetation classes (such as cropland and forest) (Fig. 5a, b). On the other hand, in arid areas, LST is not significantly related to EVI ($p > 0.05$).

3.2. Forest loss impact on land surface temperature

Fig. 6 shows the seasonal patterns of EVI and LST before and after forest loss, in three selected areas (Fig. 1). In Abobo area (Fig. 6a, b), EVI displayed a continuous decline for consecutive dry months (January–April) after forest loss occurred in 2009, while LST showed an increase of 2.2 °C for the same period. However, during wet periods (May–September), the EVI trend changed and showed an increasing pattern. LST, on the other hand, fluctuated from a decreasing (June–September) to increasing (after September) trend. Comparison of LST before and after forest loss considering all months and non-forest loss

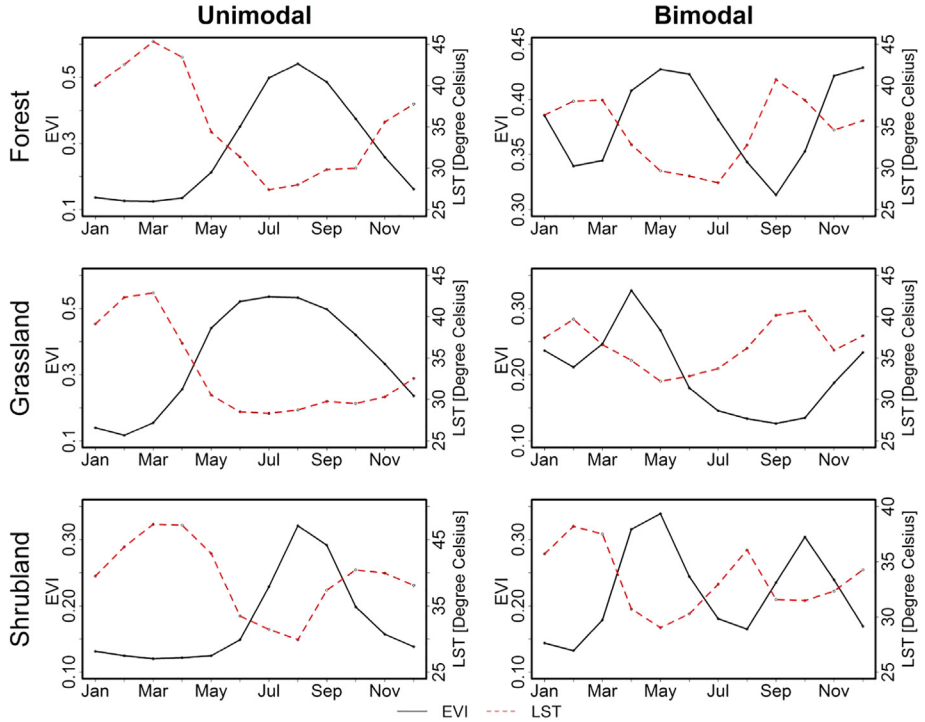

Fig. 3. Monthly mean EVI and daytime-LST for different ecoregions using 2001–2016 time series. Comparison was made using 10 × 10 km sample areas (see Fig. 2b) taken from different ecoregions where EVI–rainfall interaction was strong (correlation coefficient ≥ 0.8).

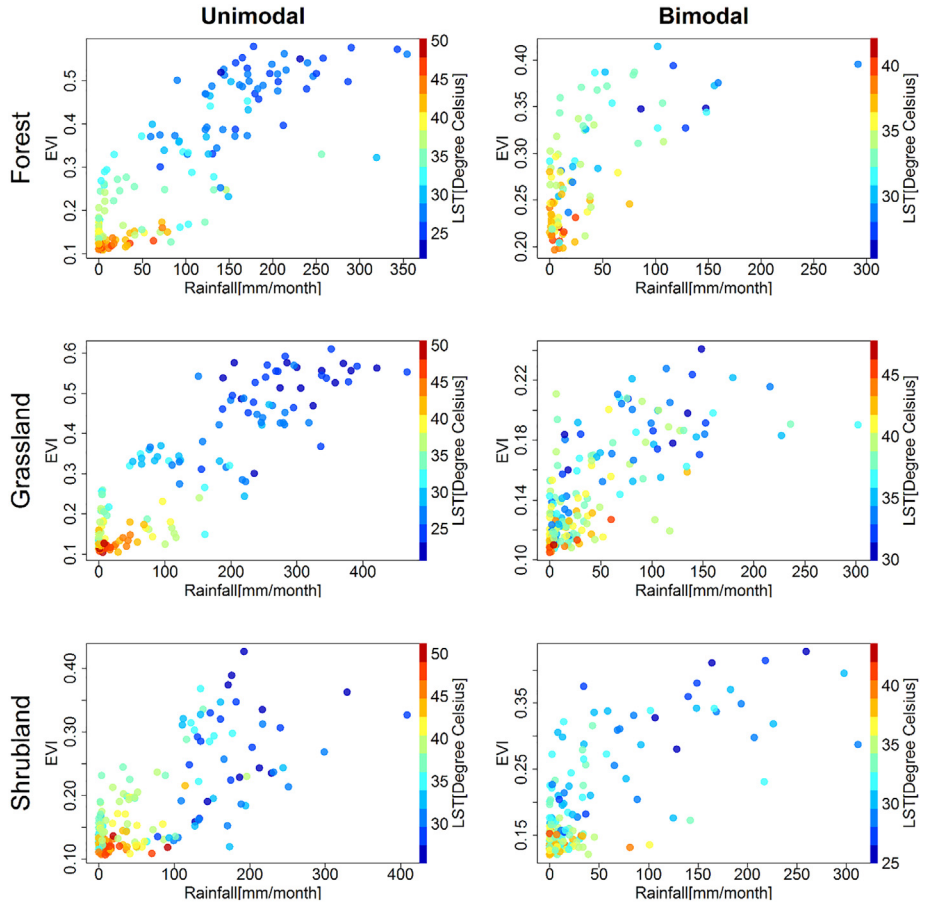

Fig. 4. EVI, rainfall, and LST interaction for different ecoregions based on 2001–2016 time series. Sample areas of 10 × 10 km (see Fig. 2c) were used for each vegetation cover type: forests, grasslands, and shrublands.

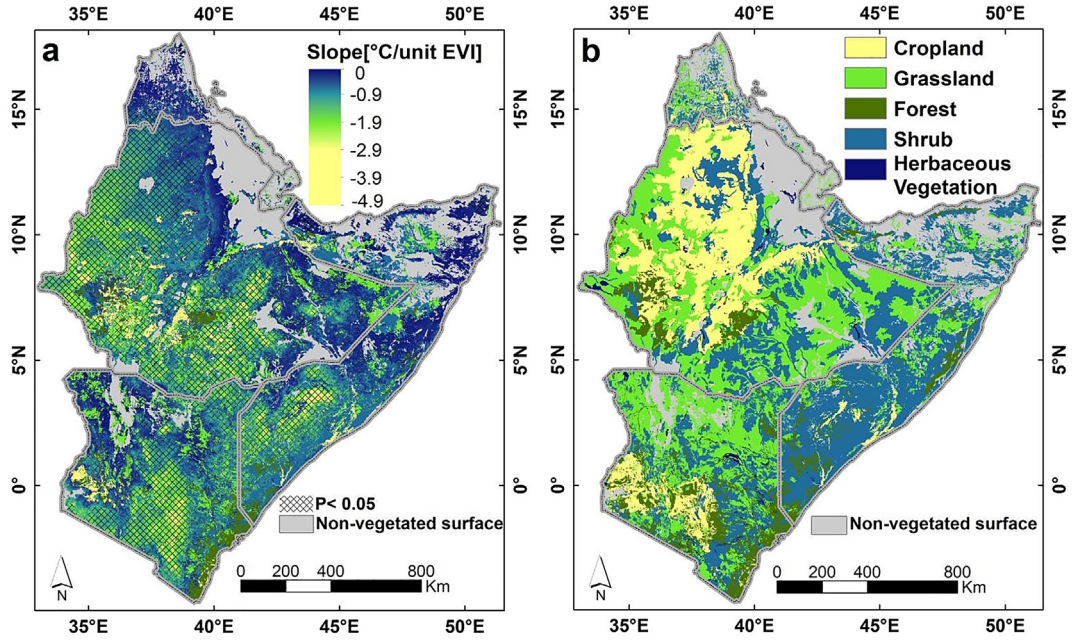

Fig. 5. a) Slope of regression between EVI (predictor variable) and LST (dependent variable) for every pixel using 2001–2016 monthly climatology data, and b) vegetation cover extracted from 2014 Global Land Cover data. Areas having significant ($p < 0.05$) EVI–LST relationship are hashed. Non-vegetated and no-data areas (due to cloud) are masked.

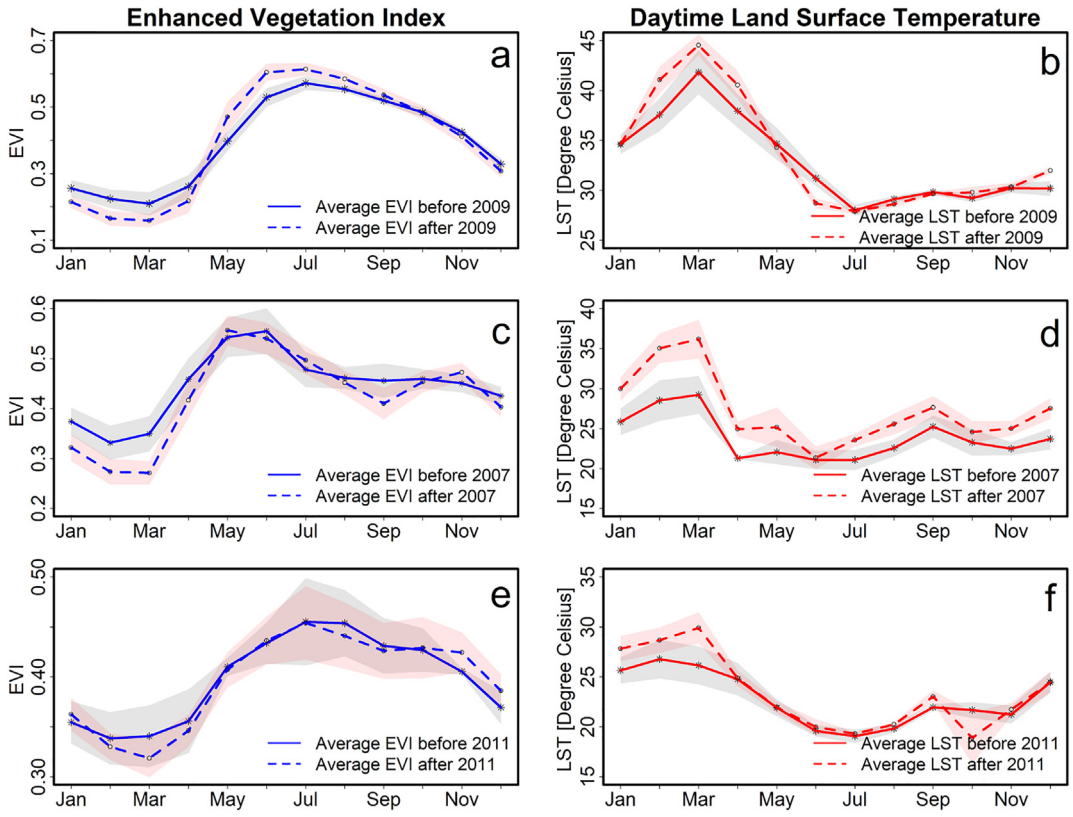

Fig. 6. Impact of forest loss on seasonality of EVI and LST for Abobo (a,b), Shakiso (c,d), and Kapcherop (e,f) areas.Shaded area indicates ± standard deviation.

signal corrections shows an average 0.68 °C increase in LST (Fig. 7a).

In Shakiso area, forest loss was observed in 2007 (Fig. 6c, d). During the dry period, EVI showed a similar declining pattern. However, in the wet period, it displayed neither significant increase nor decrease. LST, on the other hand, showed a notable and consistent increment of 2.9 °C on average throughout all months after forest loss. After removal of the non-forest loss signal due to climate variability, the area showed an overall average increase of 1.8 °C (Fig. 7b).

In Kapcherop area (Fig. 6e, f), EVI showed a similar decreasing pattern after forest loss in 2011, particularly in the dry period (February–April). LST, in contrast, displayed an average 1.98 °C increase in the same period. During the wet periods, however, both EVI and LST displayed a fluctuating trend. Taking all months into account, the area experienced an overall average increase in LST of 0.2 °C after correction (Fig. 7c).

Based on these results, dry months (December, January, February, and March) were selected to further investigate the impact of forest loss on the EVI and LST pattern. In Abobo, LST showed both negative and positive anomalies before forest loss (2009) but negative anomalies were more common (Fig. 8b). EVI, unlike LST, displayed a relatively continuous and predominantly positive anomaly for the same period (Fig. 8a). After forest loss (2009), on the other hand, LST and EVI exhibited dominantly positive and negative anomaly patterns, respectively. Evaluation of the LST and EVI patterns in the Shakiso area showed relatively distinct patterns, i.e., before forest loss LST (EVI) displayed a dominantly negative (positive) anomaly pattern (Fig. 8c, d), while after forest loss (2007) they switched their pattern, i.e., LST (EVI) displayed a dominantly positive(negative) pattern. The Kapcherop area displayed an alternating and opposite sequence of positive and negative anomaly patterns for EVI and LST before forest loss (2009), while after forest loss LST changed its pattern and displayed mainly positive anomalies consistent with Abobo and Shakiso areas (Fig. 8e, f).

3.3. Impact of drought on land surface temperature anomalies

LST anomalies caused by mild or severe droughts were significantly higher when vegetation vigor (i.e., greenness) was severely affected (i.e., EVI anomaly $< -1\sigma$) (Fig. 9; Table 2). The impact of droughts on LST anomalies decreased gradually when vegetation greenness was not affected by rainfall anomalies. In some cases, when vegetation greenness anomalies varied from zero to positive, LST anomalies could be quite small, even in severe drought conditions (Table 2). This demonstrates the strong influence of vegetation status in regulating the impact of droughts on temperature anomalies.

In the 2010 drought (October–December), in areas with mild drought (rainfall anomaly between -0.5σ and -1σ), LST anomalies consistently decreased from positive to negative as EVI anomalies increased (Fig. 9, Table 2). In regions with more severe drought (rainfall anomaly $< -1\sigma$), average LST anomalies increased considerably (1.4σ) when vegetation canopy turned brown (negative EVI anomalies). On the other hand, when EVI anomalies were positive, the effects of severe droughts on mean LST anomalies were substantially reduced (-0.7σ). The impact of vegetation greenness was more considerable in reducing warming anomalies (from 1.41 to -0.7σ) than in other drought periods.

Furthermore, while similar impacts of vegetation in reducing drought are displayed both by the 2011 and 2015 (mild and severe) drought periods (Table 2), the degree to which vegetation greening ($0–2\sigma$) suppressed the ability of severe ($< -1\sigma$) drought to cause the LST anomaly was considerably reduced from 1.57σ to 0.14σ (when EVI increased from $< -2\sigma$ to $1–2\sigma$) during June to August drought period (Fig. 9, Table 2).

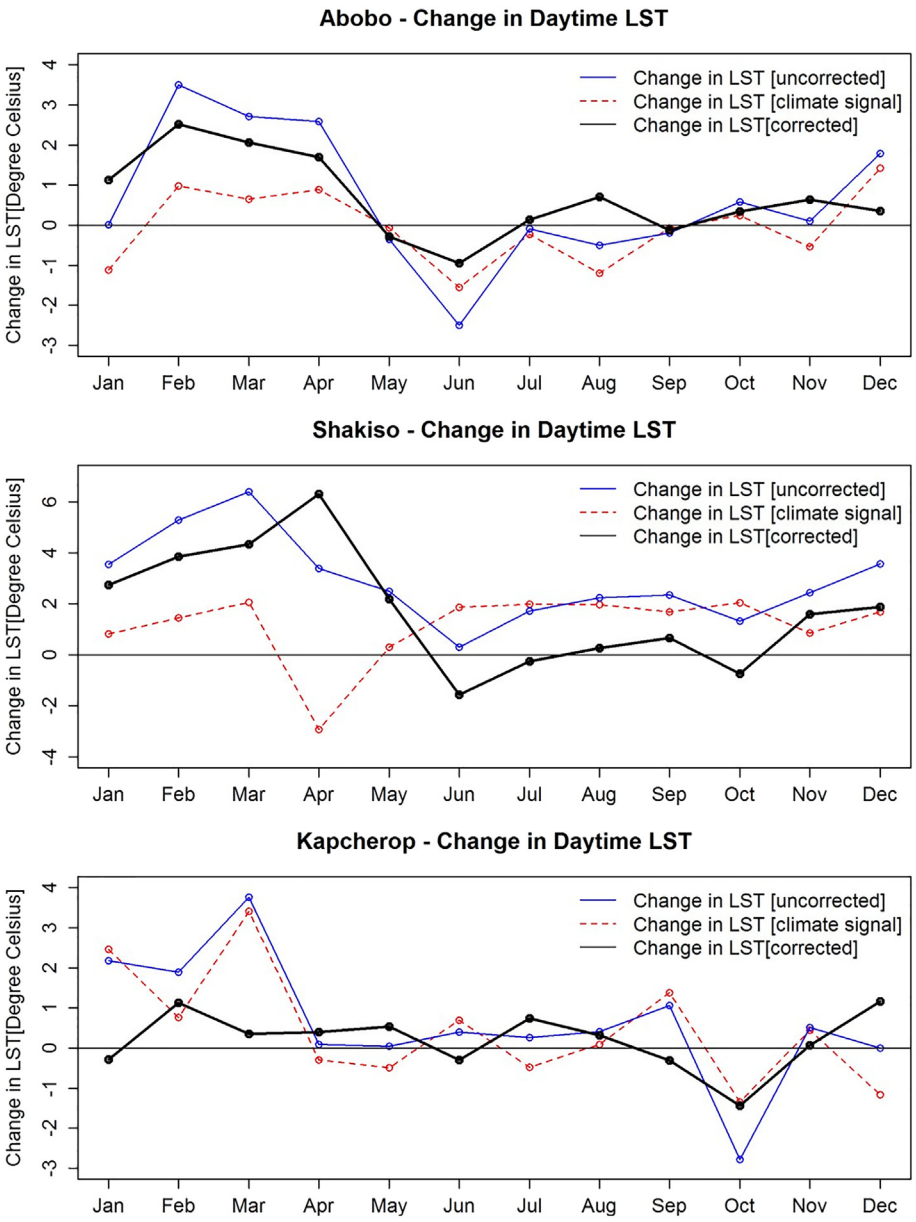

Fig. 7. Change in LST due to forest loss before and after correction for climate variability for Abobo, Shakiso, and Kapcherop areas.

4. Discussion

4.1. Rainfall–vegetation interaction and its impact on land surface temperature seasonality

The strong and positive relationship between EVI and rainfall in the region suggests that vegetation growth is primarily driven by rainfall (Fig. 2a, b). Deviations were observed along the unimodal– bimodal rainfall transition zone, where a unimodal vegetation pattern is spatially extended and changes gradually to a bimodal pattern, unlike rainfall. This is likely due to the availability of water between rainfall peak months, which supports vegetation green up. For instance, in the southwestern parts of Ethiopia, where such a case was clearly shown, the transition to a bimodal pattern is extended because the area still receives a relatively high amount of rainfall for most of the year (March–October).

Daytime LST showed a negative relationship to EVI and rainfall. However, the strength of this relationship varied with climatic zones (semi-arid and arid) and vegetation types. Semi-arid areas showed a stronger relationship than arid areas. Weak LST response in arid areas is attributed to the high radiation load and low latent heat flux associated with scarce vegetation cover and low precipitation (Rotenberg and Yakir, 2011). With respect to vegetation cover types, areas covered by grassland and shrublands, particularly in semi-arid areas, show a strong but inconsistent LST response to changes in vegetation greenness across seasons. Global studies have already indicated that LST responds to land cover change because this change can alter surface properties such as albedo, heat flux, and energy distribution (Bright et al., 2017). However, further studies are needed to clarify the inconsistent responses of LST, and other factors contributing to LST sensitivity, over various vegetation classes under stable conditions.

4.2. Impact of forest loss on land surface temperature

All three areas evaluated showed an overall warming after forest loss. The warming was particularly high and consistent during dry periods. In general, our results agree with previous studies on forest loss impact in the tropics, which have reported an increase in LST (Alkama

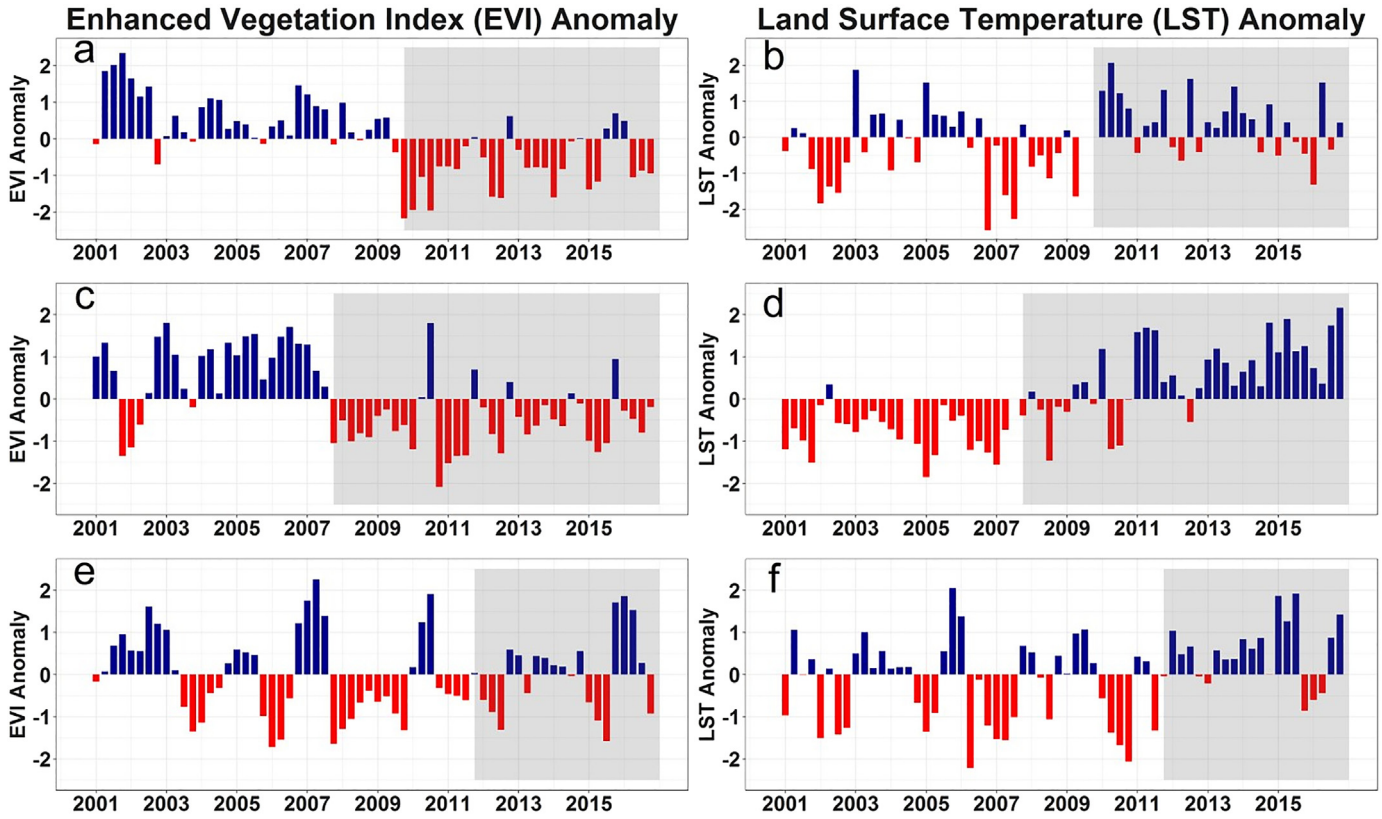

Fig. 8. EVI and LST monthly standardized anomalies before and after forest loss for dry months (January, February, March, and December) from 2001 to 2016 in Abobo (a,b), Shakiso (c,d), and Kapcherop (e,f) areas. Shaded region shows time after forest loss.

and Cescatti, 2016; Li et al., 2016). The consistent and high warming during the dry period corresponds to a decrease in EVI in all three areas (Fig. 6). The warming is likely caused by the decline in the rate of evapotranspiration and the diminishing of surface roughness together with a relatively high incoming solar radiation (insolation) during the dry periods (Sud et al., 1988; Li et al., 2016; Bright et al., 2017). In most cases across tropical regions, forest loss leads to an increase in albedo; however, the cooling effect caused by the increase in albedo is outweighed by the warming impacts caused by reduced evapotranspiration and surface roughness (Li et al., 2016). Evapotranspiration plays an important role in cooling the land surface through changing surface energy from sensible to latent heat (Schwartz and Karl, 1990). Its reduction thus leads to a rise in LST. On the other hand, surface roughness, which is affected by the height of vegetation cover, is an important factor in enhancing the exchange of sensible and latent heat fluxes and momentum between the land surface and the atmosphere through the convection of turbulent heat and convergence of moisture (Sellers et al., 1997; Sud et al., 1988). Through forest loss, this property

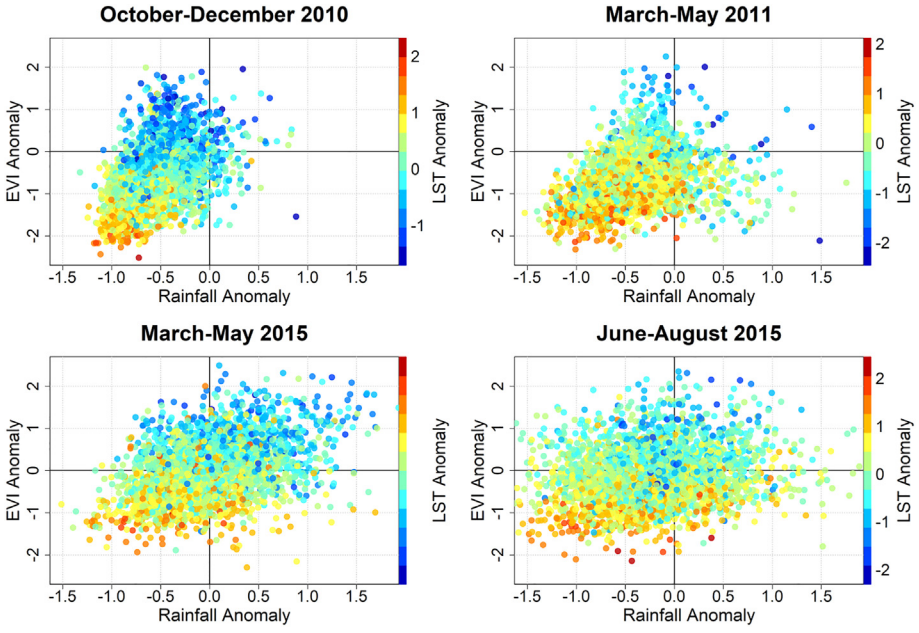

Fig. 9. Impact of rainfall – EVI interaction on LST anomalies during October–December 2010, March–May 2011, March–May 2015, and June–August 2015 drought periods. All anomalies are in units of standard deviation. Grids show bins used for calculating average LST values in Table 2. Each dot represents a pixel of 25 km in the study area. Non-vegetated pixels were excluded from analysis.

Table 2
Average LST anomaly for the EVI and rainfall anomaly bins for 2010, 2011, 2015, and 2016 drought periods.

Rainfall anomaly bin	EVI anomaly bin				
	< −2	(−2, −1)	(−1,0)	(0, 1)	(1, 2)
October–December 2010					
(0, −0.5)	Na	0.43	0.19	−0.23	−0.6
(−0.5, −1)	Na	0.83	0.51	−0.06	−0.15
< −1	1.41	0.97	0.65	−0.7	Na
March–May 2011					
(0, −0.5)	Na	0.46	0.22	−0.3	−0.81
(−0.5, −1)	Na	0.65	0.41	−0.01	−0.57
< −1	0.99	0.63	0.57	Na	Na
March–May 2015					
(0, −0.5)	Na	0.69	0.38	−0.06	−0.45
(−0.5, −1)	Na	0.79	0.42	0.05	−0.5
< −1	Na	0.89	0.57	0.34	Na
June–August 2015					
(0, −0.5)	2.09	0.82	0.51	0.15	−0.19
(−0.5, −1)	Na	0.91	0.54	0.24	−0.14
< −1	1.57	1.29	0.52	0.17	0.14

*Na = No data.

of the land surface will be suppressed leading to an amplifying impact on LST.

During the wet period, on the other hand, the lack of consistency in warming is possibly explained by the impact of the vegetation cover that replaced the forest (e.g. agricultural crops or pastures), the enhanced soil moisture, and the reduction in the incoming solar radiation flux due to clouds. High values of EVI shown during peak rainfall months after forest loss (Fig. 6a, c, e) further suggest an improvement in the evapotranspiration and surface roughness conditions, and this can possibly regulate the local climate through reducing the warming caused by forest loss during this season. When assessing the impacts of forest loss, it is important to separate changes in LST attributed to forest loss from non-forest loss climate variability. The non-forest loss signal had a diminishing role in one of the studied areas, whereas it had an exaggerating effect for the other two areas. This, however, does not change the high and consistent warming during the dry period and fluctuating patterns of warming during the wet period. Maximum LST values for the three areas were registered during the dry periods after correction for non-forest signals due to climatic variability.

4.3. The impact of drought on land surface temperature anomalies

During both severe and mild drought periods, EVI anomalies decreased significantly, while LST anomalies increased. The possible reason for the warming anomalies is the change in the radiation balance caused by the water stress. Lack of water in the soil suppresses vegetation productivity and causes browning of vegetation leading to a decline in the evapotranspiration rate. This in return slows down the dissipation of energy (from sensible to latent heat) giving rise to an increase in the sensible heat flux. Hence, with a lack of moisture in the soil and vegetation, much of the sunlight goes into raising the ground temperature.

On the other hand, the impact of drought on warming anomalies generally decreases when EVI anomalies increase from negative to positive. We showed that areas affected by the same drought severity level can show a different degree of browning and greening. This variation is likely attributed to the difference in the sensitivity and resilience among plant species because different species respond differently to drought conditions (Claussen et al., 2013). For example, drought resistant plants maintain their physiological activity for an extended period of time during droughts either by maximizing their water uptake through tapping deep water from the soil profile using their deep and dense root system or through minimizing water loss by stomatal closure and reduction of their leaf area (Kramer and Boyer, 1995; Martínez-Vilalta and Garcia-Forner, 2017; Pinheiro et al., 2005). Water stress during drought favors an increase in root size and density among deep-rooted plant species and this further enhances water uptake in times of drought stress (Ovalle et al., 2015). The ability of plants to transport water from the soil to the areas of photosynthesis is largely determined by the differences in the structure of the plant's xylem, and this property varies widely among plant species and determines the plant's ability to survive under periods of prolonged drought (Choat et al., 2012). Furthermore, Isbell et al. (2015) showed that high grassland plant diversity has increased ecosystem resistance to different degrees of drought severity and duration and suggests biodiversity can increase the resistance of ecosystem productivity to climate extremes. Hence, these differences among plant species across the study area possibly explain why some areas showed an amplified response while others remained resistant, maintaining their greening during mild drought conditions. Vegetation resilience can also be impacted by other factor such as topography. In our study area, vegetation resilience increased with elevation with the exception of March–May 2015 drought. The general increment, though, lacks consistency in particular when greening anomaly reaches peak values (i.e., EVI anomaly between 1–2σ) (Supplementary Fig. S1 and Table S1).

Further studies are necessary to clarify and identify the degree of sensitivity and resilience of various plant species to different extents of drought severity and duration in the region. This requires using high spectral-and-spatial resolution satellite, as well as ground level data, and considering additional factors, such as tree species type, density, and age. Moreover, the relation between vegetation resilience and landcover distribution (and changes) needs further investigation in the region.

5. Conclusion

In this study, we evaluated how rainfall–vegetation interactions can affect surface temperature patterns across the Horn of Africa, particularly when forest loss and extreme climatic events take place. Rainfall was shown to drive vegetation seasonality in approximately 80% of the study area, having an influence on the modality, magnitude, and timing of vegetation greening seasonal patterns. This rainfall–vegetation interplay had a strong and direct impact on LST seasonality and anomalies. An inverse relationship between vegetation greening and LST was evident across different ecosystem and bioclimatic conditions, with lower LST being observed when vegetation greening was higher. Given this relationship, forest loss was shown to considerably increase LST, particularly during dry seasons, when average LST increase due to forest loss was up to 6 °C. Forest loss also increased the frequency and magnitude of LST anomalies. Our results demonstrate that during drought events, vegetation greenness plays a crucial role in regulating LST anomalies. Even during the extreme droughts, areas where vegetation greenness were maintained could minimize or completely avoid heat stress. This highlights the importance of vegetation resilience in mitigating the impact of droughts. For instance, replacing natural vegetation by croplands or pastures, with more shallow rotting systems, creates landscapes that are more susceptible to climatic oscillations. Hence, future agricultural expansion may not only increase average LST, but will also significantly amplify heat stress during droughts. Furthermore, the increase in the frequency of droughts caused by climate change is likely to push the capacity of vegetation to maintain productivity, and consequently greenness, increasing the vulnerability of the region to extreme climatic events.

Funding

The study was supported by the Academy of Finland through project TAITAWATER - Integrated land cover-climate-ecosystem process study

for water management in East African highlands (grant number 261280); Finnish Culture Foundation through project Remote sensing of water harvesting and carbon sequestration by forests in the Taita Hills, Kenya; Ministry for Foreign Affairs of Finland through project Adaptation for Food Security and Ecosystem Resilience in Africa (grant number HEL-7670-56); University of Helsinki through project Geoinformatics for monitoring and modeling of environmental change (GIMMEC)(project number 7510203); and by the Ethiopian government under project number INSA9/AT34/1630/16.

Appendix A. Supplementary data

Supplementary data to this article can be found online at https://doi.org/10.1016/j.gloplacha.2018.05.002.

References

Alkama, R., Cescatti, A., 2016. Biophysical climate impacts of recent changes in global forest cover. Science 351 (6273), 600–604. http://dx.doi.org/10.1126/science.aac8083.

Anderson, R.G., Canadell, J.G., Randerson, J.T., Jackson, R.B., Hungate, B.A., Baldocchi, D.D., ... Halloran, T.L.O., 2011. Biophysical considerations in forestry for climate protection. Front. Ecol. Environ. 9 (3), 174–182 (Published by: Wiley on behalf of the Ecological Society of America http://www.jstor.org/stable/41149748).

Anyah, R.O., Qiu, W., 2012. Characteristic 20th and 21st century precipitation and temperature patterns and changes over the Greater Horn of Africa. Int. J. Climatol. 32, 347–363. http://dx.doi.org/10.1002/joc.2270.

Blein, R., Bwalya, M., Chimatiro, S., Faivre-Dupaigre, B., Kisira, S., Leturque, H.A.W.-Y., 2013. African Agriculture, Transformation and Outlook. NEPAD (New Partnership for African Development), pp. 72.

Bowden, J.H., Semazzi, F.H.M., 2007. Empirical analysis of intraseasonal climate variability over the Greater Horn of Africa. J. Clim. 20 (23), 5715–5731. http://dx.doi.org/10.1175/2007JCLI1587.1.

Bright, R.M., Davin, E.L., O'Halloran, T.L., Pongratz, J., Zhao, K., Cescatti, A., 2017. Local surface temperature response to land cover and management change driven by non-radiative processes. Nat. Clim. Chang. 7, 296. (Forthcoming). https://doi.org/10.1038/nclimate3250.

Brink, A.B., Eva, H.D., 2009. Monitoring 25 years of land cover change dynamics in Africa: a sample based remote sensing approach. Appl. Geogr. 29 (4), 501–512. http://dx.doi.org/10.1016/j.apgeog.2008.10.004.

Brink, A.B., Bodart, C., Brodsky, L., Defourney, P., Ernst, C., Donney, F., Tuckova, K., 2014. Anthropogenic pressure in East Africa-Monitoring 20 years of land cover changes by means of medium resolution satellite data. Int. J. Appl. Earth Obs. Geoinf. 28 (1), 60–69. http://dx.doi.org/10.1016/j.jag.2013.11.006.

Choat, B., Jansen, S., Brodribb, T.J., Cochard, H., Delzon, S., Bhaskar, R., ... Zanne, A.E., 2012. Global convergence in the vulnerability of forests to drought. Nature 4–8. http://dx.doi.org/10.1038/nature11688.

Claussen, M., Bathiany, S., Brovkin, V., Kleinen, T., 2013. Simulated climate–vegetation interaction in semi-arid regions affected by plant diversity. Nat. Geosci. 6 (11), 954–958. http://dx.doi.org/10.1038/ngeo1962.

Conway, D., Schipper, E.L.F., 2011. Adaptation to climate change in Africa : challenges and opportunities identified from Ethiopia. Glob. Environ. Chang. 21 (1), 227–237. http://dx.doi.org/10.1016/j.gloenvcha.2010.07.013.

Davin, E.L., de Noblet-Ducoudre, N., 2010. Climatic impact of global-scale deforestation: radiative versus nonradiative processes. J. Clim. 23 (1), 97–112. http://dx.doi.org/10.1175/2009JCLI3102.1.

Dutra, E., Magnusson, L., Wetterhall, F., Cloke, H.L., Balsamo, G., Boussetta, S., Pappenberger, F., 2013. The 2010–2011 drought in the Horn of Africa in ECMWF reanalysis and seasonal forecast products. Int. J. Climatol. 33 (7), 1720–1729. http://dx.doi.org/10.1002/joc.3545.

EEA-European Environment Agency, 2015. Water-Retention Potential of Europe's Forests. vol. 13 EEA Technical reporthttp://dx.doi.org/10.2800/790618.

Ellison, D., Morris, C.E., Locatelli, B., Sheil, D., Cohen, J., Murdiyarso, D., ... Sullivan, C.A., 2017. Trees, forests and water: cool insights for a hot world. Glob. Environ. Chang. 43, 51–61. http://dx.doi.org/10.1016/j.gloenvcha.2017.01.002.

Gao, X., Huete, A.R., Ni, W., Miura, T., 2000. Optical-biophysical relationships of vegetation spectra without background contamination. Remote Sens. Environ. 74 (3), 609–620. http://dx.doi.org/10.1016/S0034-4257(00)00150-4.

Goddard Earth Sciences Data and Information Services Center, 2016. TRMM (TMPA) Precipitation 1 month 0.25 degree × 0.25 degree V7. Goddard Earth Sciences Data and Information Services Center (GES DISC) (accessed February 12, 2017). http://disc.gsfc.nasa.gov/datacollection/TRMM_3B43_V7.shtml.

EM-DAT: The Emergency Events Database, Universitécatholique de Louvain (UCL) - CRED - D.Guha-Sapir-www.emdat.be, Brussels, Belgium.

Hansen, M.C., Potapov, P.V., Moore, R., Hancher, M., Turubanova, S.A., Tyukavina, A., Townshend, J.R.G., 2013. High-resolution global maps of 21st-century forest cover change. Science 342 (6160), 850–853. http://dx.doi.org/10.1126/science.1244693.

Huete, A., Didan, K., Miura, T., Rodriguez, E.P., Gao, X., Ferreira, L.G., 2002. Overview of the radiometric and biophysical performance of the MODIS vegetation indices. Remote. Sens. Environ. 83 (1), 195–213. http://dx.doi.org/10.1016/S0034-4257(02)00096-2.

Hulley, G.C., Hook, S.J., 2009. Intercomparison of versions 4, 4.1 and 5 of the MODIS land surface temperature and emissivity products and validation with laboratory measurements of sand samples from the Namib desert, Namibia. Remote Sens. Environ. 113 (6), 1313–1318. http://dx.doi.org/10.1016/j.rse.2009.02.018.

Indeje, M., Semazzi, F.H.M., Ogallo, L.J., 2000. ENSO signals in East African rainfall seasons. Int. J. Climatol. 20 (1), 19–46. http://dx.doi.org/10.1002/(SICI)1097-0088(200001)20:1<19::AID-JOC449>3.0.CO;2-0.

Isbell, F., Craven, D., Connolly, J., Loreau, M., Schmid, B., Beierkuhnlein, C., ... Eisenhauer, N., 2015. Biodiversity increases the resistance of ecosystem productivity to climate extremes. Nature 526 (7574), 574–577. http://dx.doi.org/10.1038/nature15374.

Jin, M., Dickinson, R.E., 2010. Land surface skin temperature climatology: benefitting from the strengths of satellite observations. Environ. Res. Lett. 5 (4), 44004. http://dx.doi.org/10.1088/1748-9326/5/4/044004.

Kramer, P.J., Boyer, J.S., 1995. Water Relations of Plants and Soils. Academic Press, Inc.

Latham, J., Cumani, R., Rosati, I., Bloise, M., 2014. Global Land Cover Share (GLC-SHARE) database Beta-Release Version 1.0. FAO, Rome.

Li, Y., Zhao, M., Motesharrei, S., Mu, Q., Kalnay, E., Li, S., 2015. Local cooling and warming effects of forests based on satellite observations. Nat. Commun. 6 (6603). http://dx.doi.org/10.1038/ncomms7603.

Li, Y., Zhao, M., Mildrexler, D.J., Motesharrei, S., Mu, Q., Kalnay, E., ... Wang, K., 2016. Potential and Actual impacts of deforestation and afforestation on land surface temperature. J. Geophys. Res. Atmos., 2016JD024969. http://dx.doi.org/10.1002/2016JD024969.

Ma, X., Huete, A., Moran, S., Ponce-Campos, G., Eamus, D., 2015. Abrupt shifts in phenology and vegetation productivity under climate extremes. J. Geophys. Res. Biogeosci. 120 (10), 2036–2052. http://dx.doi.org/10.1002/2015JG003144.

Martínez-Vilalta, J., Garcia-Forner, N., 2017. Water potential regulation, stomatal behaviour and hydraulic transport under drought: deconstructing the iso/anisohydric concept. Plant Cell Environ. 40 (6), 962–976. http://dx.doi.org/10.1111/pce.12846.

Meroni, M., Rembold, F., Fasbender, D., Vrieling, A., 2017. Evaluation of the Standardized Precipitation Index as an early predictor of seasonal vegetation production anomalies in the Sahel. Remote Sens. Lett. 8 (4), 301–310. http://dx.doi.org/10.1080/2150704X.2016.1264020.

NASA LP DAAC, 2014. MCD43B1 BRDF-Albedo Model Parameters 8-Day L3 Global 1km Version 5. NASA EOSDIS Land Processes DAAC, USGS Earth Resources Observation and Science (EROS) Center, Sioux Falls, South Dakota , Accessed date: 10 December 2016.

Nicholson, S.E., 1996. A review of climate dynamics and climate variability in Eastern Africa. In: Johnson, T.C., Odada, E.O. (Eds.), The Limnology, Climatology and Paleoclimatology of the East African Lakes. Gordon and Breach, Amsterdam, pp. 25–56 (63–75).

Ovalle, J.F., Arellano, E.C., Ginocchio, R., 2015. Trade-offs between drought survival and rooting strategy of two South American Mediterranean tree species: implications for dryland forests restoration. Forests 6 (10), 3733–3747. http://dx.doi.org/10.3390/f6103733.

Pellikka, P.K.E., Clark, B.J.F., Gosa, A.G., Himberg, N., Hurskainen, P., Maeda, E., ... Siljander, M., 2013. Agricultural expansion and its consequences in the Taita Hills, Kenya. Dev. Earth Surf. Process. 16 (2006), 165–179. http://dx.doi.org/10.1016/B978-0-444-59559-1.00013-X.

Peng, S.-S., Piao, S., Zeng, Z., Ciais, P., Zhou, L., Li, L.Z.X., ... Zeng, H., 2014. Afforestation in China cools local land surface temperature. Proc. Natl. Acad. Sci. 111 (8), 2915–2919. http://dx.doi.org/10.1073/pnas.1315126111.

Pinheiro, H.A., DaMatta, F.M., Chaves, A.R.M., Loureiro, M.E., Ducatti, C., 2005. Drought tolerance is associated with rooting depth and stomatal control of water use in clones of Coffeacanephora. Ann. Bot. 96 (1), 101–108. http://dx.doi.org/10.1093/aob/mci154.

Rotenberg, E., Yakir, D., 2011. Distinct patterns of changes in surface energy budget associated with forestation in the semiarid region. Glob. Chang. Biol. 17 (4), 1536–1548. http://dx.doi.org/10.1111/j.1365-2486.2010.02320.x.

Schwartz, M.D., Karl, T.R., 1990. Spring phenology: Nature's experiment to detect the effect of "green-up" on surface maximum temperatures. Mon. Weather Rev. http://dx.doi.org/10.1175/1520-0493(1990)118<0883:SPNETD>2.0.CO;2.

Scott, D.F., 2005. The hydrological and soil impacts of forestation in the tropics. In: Forests, Water and People in the Humid Tropics. Cambridge University Press, pp. 622–651 Published by.

Sellers, A.P.J., Dickinson, R.E., Randall, D.A., Betts, A.K., Hall, F.G., Berry, J.A., ... Field, C.B., 1997. Modeling the exchanges of energy, water, and carbon between continents and the atmosphere. Published by: American Association for the Advancement of Science Stable URL. http://www.jstor.org/stable/2891797Science 275 (5299), 502–509. http://dx.doi.org/10.1126/science.275.5299.502.

Sud, Y.C., Shukla, J., Mintz, Y., 1988. Influence of land surface roughness on atmospheric circulation and precipitation: a sensitivity study with a general circulation model. J. Appl. Meteorol. http://dx.doi.org/10.1175/1520-450(1988)027<1036:IOLSRO>2.0.CO;2.

USGS EDC DAAC, 2016. U.S. Geological Survey. EROS Data Center Distributed Active Archive Center (EDC DAAC), Sioux Falls, South Dakota. https://earthexplorer.usgs.gov.

Wan, Z.S.H., 2015. MOD11A2 MODIS/Terra Land Surface Temperature/Emissivity 8-Day L3 Global 1km SIN Grid V006. NASA EOSDIS Land Processes DAAC. http://dx.doi.org/10.5067/modis/mod11a2.006.

White, F., 1983. The vegetation of Africa: a descriptive memoir to accompany the UNESCO/AETFAT/UNSO vegetation map of Africa. Nat. Resour. Res. 20. http://dx.doi.org/10.2307/2260340.

Williams, A.P., Funk, C., 2011. A westward extension of the warm pool leads to a westward extension of the Walker circulation, drying eastern Africa. Clim. Dyn. 37 (2011), 2417–2435. http://dx.doi.org/10.1007/s00382-010-0984-y.

Zhao, M., Running, S.W., 2010. Drought-induced reduction in global terrestrial net primary production from 2000 through 2009. Science 329 (5994), 940–943. http://dx.doi.org/10.1126/science.1192666.